9A.2 STATISTICAL REPRESENTATION OF EQUATORIAL WAVES AND TROPICAL INSTABILITY WAVES IN THE PACIFIC OCEAN

Toshiaki Shinoda[1,2]*, George N. Kiladis[3] and Paul E. Roundy[4]

[1]Naval Research Laboratoty
[2]Planning Systems Inc.
[3]NOAA Earth System Research Laboratory
[4]University at Albany, State University of New York,

1. Introduction

Equatorially-trapped waves account for a large portion of the intraseasonal variability in the tropical atmosphere and ocean, and play an important role in driving a variety of longer time scale phenomena (e.g., ENSO). Kelvin, Rossby and Mixed Rossby-Gravity waves corresponding to the eigenmodes of the linearized shallow water equations of Matsuno (1966) have been shown to be of particular importance in the equatorial Pacific ocean. While oceanic equatorial waves have been identified in in-situ data (e.g. Johnson and McPhaden 1993) and in satellite altimeter data (e.g., Miller et al. 1988, Delcroix et a. 1991, Boulanger and Fu 1996, Chelton et al. 2003) their observed dispersion relationships have not yet been fully described in frequency-wavenumber space. A recent study by Wakata (2007) demonstrated that the dispersion relations of equatorial Rossby and Kelvin waves could be inferred from satellite data by frequency-wavenumber spectra of sea surface height (SSH). However, because his analysis includes the background spectrum, it is difficult to compare the spectral signal with theoretical dispersion curves especially in the high wavenumber domain. In this study, frequency-wavenumber spectral analysis will be applied to identify observed dispersion relations of oceanic equatorial waves using sea surface height data measured by satellite altimetry.

It is found that signals of oceanic Kelvin and equatorial Rossby waves are evident in the frequency-wavenumber spectrum of SSH. The same analysis is also conducted using sea surface temperature (SST), showing a prominent spectral peak in both SSH and SST at frequencies and wavenumbers consistent with those of tropical instability waves (TIWs). Further statistical analyses are conducted to isolate the structure of TIWs.

*Corresponding author address: Toshiaki Shinoda, Naval Research Laboratory, Stennis Space Center MS 39529

2. Data

Four primary data sets are used in this study. 10-day average SSH data derived from TOPEX altimetry are used to identify signals of equatorial waves and TIWs. Data for the 10-year period of 1993-2002 with horizontal resolution of 1° are analyzed. Weekly SSTs from the analysis of Reynolds et al. (2002) are used to provide a statistical description of SST variability associated with TIWs and to examine the interannual variation of TIW activity. Data for the period 1982-2005 with 1° horizontal resolution are analyzed. The TRMM Microwave Imager (TMI) SST for a period 1998-2005 are also analyzed to describe the structure of TIWs. The 3-day average TMI SST data are originally gridded at 0.25°x 0.25°. We average the data onto a 1° x 1° grid for comparison with the Reynolds SST. 1° resolution is considered sufficient since the typical wavelength of TIWs is ∼1500 km. Near surface velocity data derived from the Ocean Surface Current Analysis-Real time (OSCAR) project (Lagerloef et al. 1999, Bonjean and Lagaloef, 2002) are used to statistically describe the structure of surface current anomalies associated with TIWs. The 5-day average near surface velocity fields on 1°x 1° grid are estimated using SSH data from 1999-2005 satellite altimeter measurements, surface wind stress, and drifter data.

Since the OSCAR velocity is not derived from direct current measurements at each grid point, it is necessary to compare the data with other direct

measurements, especially near the equator where geostrophic balance does not necessarily hold. Bonjean and Lagaerloef (2002) compared the OSCAR velocity with direct measurements from TOGA TAO buoys for annual and interannual variations, showing that the OSCAR data can well capture these variations on the equator especially in the eastern Pacific. In this study, we also examined the subseasonal variability of OSCAR velocity.

The 5-day average zonal velocity at 10m from TAO measurements at 140°W, equator during September 2001-December 2005 is compared with the surface zonal velocity from OSCAR (not shown). The results indicate that the OSCAR velocity agrees well with TAO data (correlation coefficient=0.66) including subseasonal velocity fluctuations associated with strong TIW activity such as was observed during November-December 2001 (Cronin et al. 2002) and August-September 2004 (Jochum et al. 2007). The reasonable agreement suggests that the OSCAR velocity data are suitable for the statistical description of TIW structures.

3. Frequency-wavenumber spectral analysis

Wheeler and Kiladis (1999) demonstrated that wavenumber-frequency spectral analysis is useful for identifying signals of atmospheric equatorial waves, and for isolating their structure. Also, wavenumber-frequency spectral analysis was recently used to identify oceanic equatorial waves in numerical model experiments (Shinoda et al. 2008). In this section, the same technique used in Wheeler and Kiladis (1999) is applied to the satellite-derived SSH to examine to identify oceanic equatorial waves.

Figure 1a shows contours of the base 10 logarithm of power in the wavenumber-frequency space calculated using SSH anomalies in the equatorial area (5°N-5°S) in the Pacific Ocean. Prominent spectral signals of the equatorial Kelvin wave are evident, with their peak corresponding to a phase speed of 2.8 m/s, consistent with the first baroclinic mode. Also, in the negative (westward) wavenumber domain, a spectral peak close to the dispersion curve of the equatorial Rossby wave is evident. In particular, a peak at a period of ∼33 days and wavenumber ∼1500 km on the dispersion curves is prominent. These frequencies and wavenumbers are consistent with those associated with TIWs (e.g., Qiao and Weisberg 1995, Weidman et al. 1999, Lyman et al., 2007).

While many previous studies discussed the structure of ∼33 day period TIWs, Lyman et al. (2007) recently detailed the structure of TIWs with a 17-day period. The peak around 17 days could potentially affect the spectrum at longer periods through aliasing. A 33-day spectral peak can be contaminated by aliasing only if there is significant power at ∼14 days given the sampling is 10 days. Since Lyman et al. (2007) show that power less than 15 days is nearly zero (see their Fig. 14), it is unlikely that the 33-day peak is significantly influenced by 17-day signals through aliasing.

Figure 1b shows the spectrum calculated from the same analysis using the TMI SST. While there is no significant peak near the Kelvin wave dispersion curve, a peak at ∼33 days and wavenumber ∼1500 km is once more evident, suggesting again a spectral signal associated with TIWs. A similar peak is found in the Reynolds SST, showing that significant portion of TIW variability can be captured by the weekly SST analysis (Fig. 1c).

In order to describe the spatial variation of TIW activity, space and time filtering (via spectral transform) centered around the spectral peak (the area of rectangle in Fig. 1c) is applied to the time series of SSH and SST. Figure 2a, 2b, and 2c show the variance of filtered time series at each location from SSH, TMI SST and Reynolds SST respectively. The maximum of SSH fluctuation associated with TIWs is found at 5°N, 130°W, while the maximum in the SST signal is found around 2°N, 120°W (Fig. 2a and 2b). A similar spatial pattern is found in the analysis of Reynolds SST, but the overall amplitude is weaker (Fig. 2c).

4. Cross correlation analysis

Previous observational studies indicate that TIWs are generally associated with strong fluctuations of SST, SSH and near surface velocity (e.g., Duing et al. 1975, Legeckis, 1977, Miller et al. 1985, Kennan and Flament 2000, Polito et al. 2001, Chelton et al, 2003). In this section, the phase relationships between SST, SSH and surface velocity are described statistically using long records based on a cross correlation analysis.

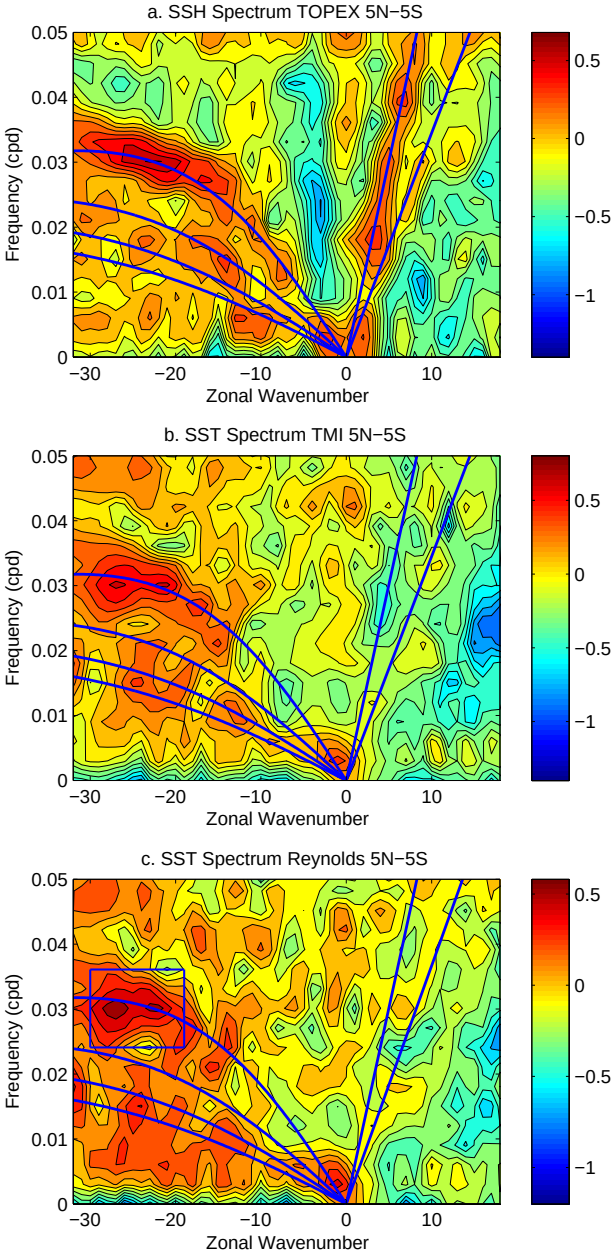

Figure 1: Zonal wavenumber-frequency power spectra of SSH anomalies from TOPEX (a), from SST anomalies from TMI SST (b), and from Reynolds SST (c). The straight lines indicate 2.8 m/s and 1.6 m/s phase lines. Curves in the negative wavenumber domain is Rossby wave dispersions of first 4 meridonal modes with the same equivalent depth of 2.8 m/s Kelvin wave.

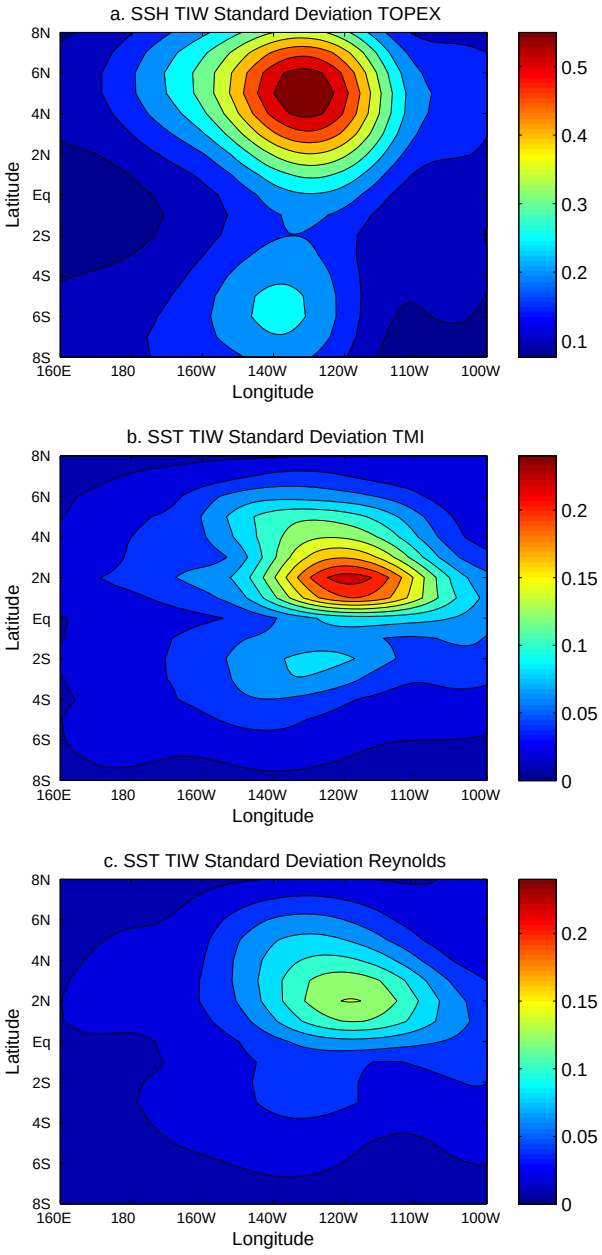

Figure 2: (a) Variance of SSH anomalies filtered at periods 28-41 days and wave lengths 1336-2109 km (see the rectangle in Fig. 2c) (b) Same as (a) except for SST anomalies from TMI. (c) Same as (a) except for SST anomalies from Reynolds SST.

Time series of unfiltered SSH, SST, and surface current anomalies are regressed against space and time filtered TIW SSH anomalies at 5°N, 130°W

where the amplitude is maximum in Fig. 2a. The data for the period 1999-2002, during which all data sets are available, are used for the analysis. Figure 3a shows the relationship of these variables using TMI SST. Maximum SST anomalies are located around 2°N, extending to the northeast. Maximum SSH anomalies are found around 5°N, which corresponds to the local maximum of SST anomalies around this latitude. Surface velocity is found to be almost parallel to the contour lines of SSH, showing nearly geostrophic balance. Because the maximum SSH anomalies are located on the northeast side of the maximum SST anomalies, northward (southward) current anomalies are found at the coldest (warmest) anomalies around 2°N, causing a net meridional heat transport. While these SST anomalies are initially advected by velocity fluctuations caused by barotropic instability from the cyclonic shear between the South Equatorial Current and North Equatorial Countercurrent or Equatorial Undercurrent (e.g., Qiao and Weisberg 1998, Contreras 2002, Chelton et al. 2003), it is possible that variation of temperature front may influence the evolution of TIWs given that the surface velocity fields are nearly geostrophic balance.

On the equator, the maximum westward (eastward) currents are found where the zonal gradient of SST anomalies is positive (negative), corresponding to a strong zonal advection of heat. This result is consistent with the analysis of TOGA TAO data (Jochum et al. 2007). The SSH signal is small on the equator, consistent with previous studies (e.g., Musman et al. 1989). These features are also evident in the Reynolds SST, but their amplitude is about 2/3 of that in TMI SST (Fig. 3b).

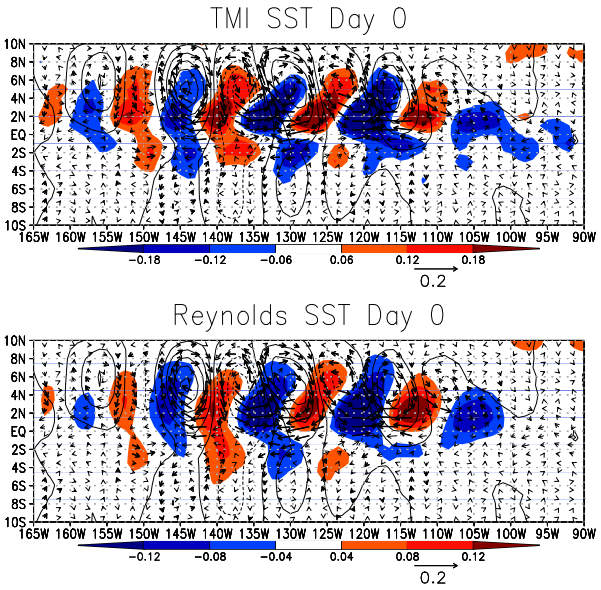

Figure 3: Upper panel: SST (shading), SSH (contour), and surface current (arrows) anomalies regressed onto space and time filtered SSH anomalies at 5°N, 130°W. TMI SST is used for the analysis. The contour interval is 0.2 cm. The solid (dashed) contour indicates positive (negative) values. Thick arrows indicate velocities larger than 0.03 m/s. Lower panel: Same as the upper panel except Reynolds SST is used.

5. Conclusions

Satellite derived SSH, SST and surface velocity are analyzed to examine oceanic equatorial waves and tropical instability waves. Signals of oceanic equatorial waves can be isolated by frequency wavenumber spectral analysis of SSH fields derived from satellite altimeter measurements. The prominent peak around 33 days and 1500 km is found to be associated with TIWs. Salient features of TIWs such as phase relationships between surface velocity, SSH, and SST can be effectively isolated by a combination of frequency wavenumber spectral analysis and regression.

References

Bonjean F. and G.S.E. Lagerloef, 2002: Diagnostic Model and Analysis of the Surface Currents in the Tropical Pacific Ocean. J. Phys. Oceanogr., 32, 2938-2954.

Boulanger, J.-P., and L.-L. Fu, 1996: Evidence of boundary reflection of Kelvin and first-mode Rossby waves from TOPEX/POSEIDON sea level data. J. Geophys. Res., 101, 16361-16371.

Chelton, D. B., M. G, Schlax, J. M. Lyman, and G. C. Johnson 2003: Equatorially trapped Rossby waves in te presence of mreidionally sheared baroclinc flow in the Pacific Ocean. Prog. Oceanogr., 56, 323-380

Contreras, R. F., 2002: Long-term observations of tropical instability waves. J. Phys. Oceanogr., 32, 2715-2722.

Cronin, M. F., S.-P. Xie, and H. Hashizume 2003: Barometric pressure variations associated with eastern Pacific tropical instability waves. J. Climate, 16, 3050-3057.

Delcroix, T., J. Picaut, and G. Eldin, 1991: Equatorial Kelvin and Rossby wave evidenced in the Pacific Ocean through Geosat sea level and surface current anomalies. J. Geophys. Res., 96, 3249-3262.

Duing, W., P. Hisard, E. Katz, J. Knauss, J. Meincke, L. Miller, K. Moroshkin, G. Philander, A. Rybnikov, K. Voigt, R. Weisberg., 1975: Meanders and longwaves in the equatorial Atlantic. Nature, 257, 280-284.

Jochum, M., M. F. Cronin, W. S. Kessler, and D. Shea, 2007: Observed horizontal temperature advection by tropical instability waves. Geophyis. Res. Lett., in press.

Kennan, S. C., P. Flament, 2000: Observations of tropical instability vortex. J. Phys. Oceanogr., 30, 2277-2301.

Lagerloef G.S.E., G.T. Mitchum, R. Lukas, and P.P. Niiler, 1999: Tropical Pacific near Surface Currents estimated from altimeter, wind and drifter data. J. Geophys. Res., 104, 23 313-23 326.

Legeckis, R. V., 1977: Long waves in th eastern equatorial ocean. Science, 197, 1177-1181.

Lyman, J. M., G. C. Johnson, and W. S. Kessler, 2007: Distinct 17- and 33-Day Tropical Instability Waves in Subsurface Observations. J. Phys. Oceanogr.,37, 855-872.

Matsuno, T., 1966: Quasi-geostrophic motions in the equatorial area. J. Meteor. Soc. Japan, 44, 25-43.

Miller, L., D. R. Watts, and M. Wimbush, 1985: Oscillations of dynamic topography in the eastern Pacific. J. Phys. Oceanogr., 15, 1759-1770.

Miller, L., R. Cheney, and B. Douglas, 1988: GEOSAT altimeter observations of Kelvin waves and the 1986-87 El Nino. Science, 239, 52-54.

Musman, S. 1989: Sea height wave form in equatorial waves and its interpretation. J. Geophys. Res., 94, 3303-3309.

Polito, P. S., J. P. Ryan, W. T. Liu, F. P. Chavez, 2001: Oceanic and atmospheric anomalies of tropical instability waves. Geophys. Res. Lett., 28, 2233-2236.

Qiao, L., and R. H. Weisberg, 1995: Tropical instability wave kinematics: Observations from the Tropical Instability Wave Experiment (TIWE). J. Geophys. Res., 100, 8677-8693.

Reynolds, R.W., N.A. Rayner, T.M. Smith, D.C. Stokes, and W. Wang, 2002: An improved in situ and satellite SST analysis for climate. J. Climate, 15, 1609-1625.

Shinoda, T., P. E. Roundy, and G. N. Kiladis, 2008: Variability of intraseasonal Kelvin waves in the equatorial Pacific Ocean. J. Phys. Oceanogr., (in press).

Wakata, Y., 2007: Frequency-Wavenumber Spectra of Equatorial Waves Detected from Satellite Altimeter Data. J. Oceanogr., 63, 483-490.

Weidman, P. D., D. L. Mickler, B. Dayyani Et, and G. H. Born, 1999: Analysis of Legeckis eddies in the near-equatorial Pacific. J. Geophys. Res., 104, 7865-7887.

Wheeler, M., and G. N. Kiladis, 1999: Convectively coupled equatorial waves: Analysis of clouds and temperature in the wavenumber-frequency domain. J. Atmos. Sci., 56, 374-399.